ACS OMEGA

Article

Cite This: ACS Omega 2018, 3, 12893−12904

http://pubs.acs.org/journal/acsodf

Push−Pull *N,N*-Diphenylhydrazones Bearing Bithiophene or Thienothiophene Spacers as Nonlinear Optical Second Harmonic Generators and as Photosensitizers for Nanocrystalline TiO_2 Dye-Sensitized Solar Cells

Sara S. M. Fernandes,[†] Michael Belsley,[‡] Ana I. Pereira,[§] Dzmitry Ivanou,[§] Adélio Mendes,[§] Licínia L. G. Justino,[∥] Hugh D. Burrows,[∥] and M. Manuela M. Raposo*[,†]

[†]Centro de Química and [‡]Centro de Física, Universidade do Minho, Campus de Gualtar, 4710-057 Braga, Portugal

[§]LEPABE—Faculdade de Engenharia, Universidade do Porto, rua Dr. Roberto Frias, 4200-465 Porto, Portugal

[∥]Centro de Química de Coimbra (CQC), Departamento de Química, Universidade de Coimbra, P3004-535 Coimbra, Portugal

Supporting Information

ABSTRACT: A series of push−pull heterocyclic *N,N*-diphenylhydrazones were prepared to study the effect of structural modifications (different π-spacers and electron-withdrawing groups) on the optical (linear and nonlinear) and electronic properties of the molecules. The photovoltaic response of dye-sensitized solar cells assembled using nanocrystalline titania photosensitized with the synthesized dyes was also studied. These heterocyclic push−pull conjugated dyes involve *N,N*-diphenylhydrazones as electron donors linked to bithiophene or thieno[3,2-*b*]thiophene spacers and were functionalized with carboxylic acid, cyanoacetic acid, or dicyanovinyl acceptor groups. A combination of Suzuki−Miyaura cross-coupling, Vilsmeier formylation, and condensation reactions was used to synthesize the intermediates and final products. Density functional theory (DFT) and time dependent-DFT calculations were used to obtain information on conformation, electronic structure, and electron distribution, both for the free dyes and those adsorbed on TiO_2. The results of this multidisciplinary study indicate that dyes **5b** and **6b** have the strongest second-order nonlinear optical response with hyperpolarizability values in the range of $\beta = 2330 \times 10^{-30}$ to 2750 $\times 10^{-30}$ esu, whereas photovoltaic power conversion efficiencies reach values in the range of 0.7−3.0% for dyes **5a−b** and **7c** and were enhanced by coadsorbing deoxycholic acid (0.8−5.1%).

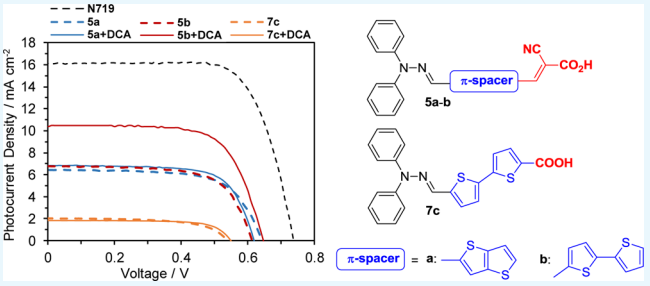

1. INTRODUCTION

Push−pull heteroaromatic π-conjugated systems are established compounds in materials science, which combine easy synthesis with tunability of structures to produce systems with predictable and unique optoelectronic properties. The molecular arrangement of these D−π−A systems leads to terminal electron donor and acceptor group communication through a π-conjugated bridge. This intramolecular charge transfer (ICT) involves a new low-energy molecular orbital, accessible through visible light excitation, which is responsible for the polarization of the molecule.[1,2]

Optoelectronic properties of these push−pull systems may have applications in field-effect transistors,[3] light-emitting diodes,[4] nonlinear optics [second harmonic generation (SHG) and two-photon absorption],[5−7] photovoltaics,[8−13] and near-infrared absorbing dyes.[14]

These push−pull systems may be tailored toward specific applications by changing electron donor or acceptor moieties, spacer (conjugation length, planarity, and electronic nature), and the overall chromophore arrangement. An efficient method of tuning the electronic properties of these systems involves incorporation of heterocyclic units, which provide high polarizability, thermal and chemical robustness, and possibilities for further structural changes. In addition, they can behave as both efficient spacers and auxiliary electron donor/acceptor groups. A variety of π-bridges and donor and acceptor groups have been used in the design of heterocyclic push−pull heterocyclic dyes.[1,2]

Aromatic hydrazone-based compounds have been studied in several areas of materials chemistry, such as organic nonlinear optical (NLO)[15−18] and hole-transport materials, and so forth.[19,20] These compounds have been of particular interest because of the easy synthetic access through reaction of carbonyl compounds (particularly aldehydes) with relatively low-cost starting materials, avoiding expensive catalysts. They are also tolerant to the presence of water and/or oxygen. Other

Received: May 25, 2018
Accepted: July 27, 2018
Published: October 9, 2018

DOI: 10.1021/acsomega.8b01045
ACS Omega 2018, 3, 12893−12904

Scheme 1. Synthesis of *N,N*-Diphenylhydrazone Derivatives 3−7: (i) EtOH, rt; (ii) DMF, $POCl_3$; (iii) 2-Cyanoacetic Acid, EtOH, Piperidine, Reflux; and (iv) Malononitrile, EtOH, Piperidine, Reflux

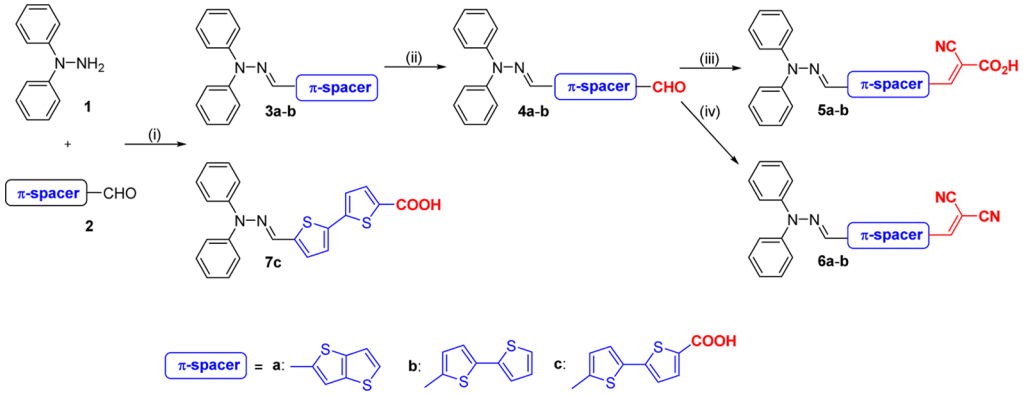

interesting characteristics are the extended conjugation when compared to the corresponding amines, good thermal and chemical stability, and enhancement of charge mobility through delocalization of the terminal nitrogen atom lone pair into the π-conjugated system.[16−20]

Although application of compounds with a hydrazone moiety as efficient electron donors in bulk-heterojunction solar cells has previously been reported,[21−23] few have been studied as sensitizing dyes for nanocrystalline TiO_2 dye-sensitized solar cells (DSSCs).[24−28] The excellent electronic properties of the thiophene moiety have led to its widespread application in the design of ICT chromophores.[29,30]

On the basis of the interesting results reported by us and other groups[1,2,15−18,24−28] on push−pull heterocyclic π-conjugated systems for NLO[31−41] and photovoltaic applications,[42−45] we have synthesized five organic dyes bearing electron-rich heteroaromatic groups (*N,N*-diphenylhydrazone and thiophene) as the donor moiety or/π-spacer and carboxylic, cyanoacetic acid, or dicyanovinyl moieties as the strong electron-withdrawing/-anchoring groups. Their optical and redox properties have been evaluated, and they have been tested in DSSC photovoltaic devices.

2. RESULTS AND DISCUSSION

2.1. Synthesis and Characterization. A series of push−pull heterocyclic chromophores were prepared to study the effect of different spacers (bithiophene and thieno[3,2-*b*]thiophene) and electron-withdrawing moieties (carboxylic acid, cyanoacetic acid, and dicyanovinyl) on their linear and NLO properties, redox behavior, and potential as sensitizers in DSSCs based on nanocrystalline titania. All of the compounds bear a *N,N*-diphenylhydrazone donor unit that was chosen because of its high charge mobility properties as an electron donor.[25] The thiophene units in the π-spacer show excellent charge-transfer properties, efficient π-conjugation, and low geometrical relaxation upon oxidation.[29,31−47]

The aldehyde precursor **2c** was prepared in good yield (53%) by Suzuki−Miyaura cross-coupling of 5-bromothiophene-2-carboxylic acid and 5-formyl-2-thiopheneboronic acid. Intermediates **3a−b** and push−pull chromophore **7c** were synthesized in moderate to good yields (55−72%) through condensation of the respective aldehydes **2a−c** with *N,N*-diphenylhydrazone **1** in ethanol. The intermediate aldehydes **4a−b** were obtained (45−58% yields) by Vilsmeier−Haack formylation. Knoevenagel condensation (piperidine catalyst) in refluxing ethanol of the aldehydes **4a−b** with 2-cyanoacetic acid gave the push−pull chromophores **5a−b** in fair to good yields (27−58%), whereas dyes **6a−b** were prepared in fair yields (22−29%) by condensation of the same aldehydes with malononitrile (Scheme 1).

Recently, the synthesis of precursor **3a** was reported by Roncali and collaborators through condensing *N,N*-diphenylhydrazine with aldehyde **2a**, in 63% yield, using different experimental conditions: MeOH/tetrahydrofuran in the presence of sodium acetate. Aldehyde **4b** was also reported, in 37% yield, using a one-step methodology by condensing *N,N*-diphenylhydrazine with 5,5′-diformylbithiophene. The same investigators also published the synthesis of dyes **6a−b** using different reaction conditions (NET_3 as the base and $CHCl_3$ as the solvent).[23]

The structures of these compounds were confirmed by standard procedures (detailed characterization and Table S1 with experimental data in the Supporting Information).

2.2. Electrochemical Study. To obtain energies of highest occupied molecular orbital (HOMO) and lowest unoccupied molecular orbital (LUMO) redox properties of the compounds, **5a−b** and **7c** were studied using cyclic voltammetry (CV). In DSSCs, dye **N719** is most commonly used; its band gap energy is appropriate for absorption in the visible region of the solar spectra; energies of LUMO and HOMO fit well for electron injection into TiO_2 and regeneration of the dye. Data on the electrochemical behavior of **N719** are presented as a "reference". The energies of HOMO and LUMO of **5a−b** and **7c** were calculated. The energy level of ferrocene (4.39 eV) was used as the reference. Table 1 summarizes the data. For compounds **5** and **7**, the redox behavior is reversible; whatever scan rate of potential is applied, the potentials of cathodic and anodic peaks of current remain constant. Potentials for oxidation of compounds **5a**, **5b**, and **7c** are 0.73, 0.67, and 0.64 V, respectively. These potentials are higher than the potential of the $3I^-/I_3^-$ couple (0.42 V), which in the case of application in solar cells, reduces back transfer of electrons to the electrolyte.[48,49] The oxidation potential clearly depends on the electronic nature of the heteroaromatic spacer unit: the stronger the auxiliary electron-donating ability, the easier it is to oxidize the molecule. The bithiophene derivative **5b** displays the lowest oxidation potential (highest energy of HOMO), suggesting a slightly stronger electron-donating ability when compared to compound **5a** (this is in accordance with the UV−vis spectral data). The LUMO level of the dyes indicates the thermodynamic possibility of the electron injection into the conduction band of TiO_2 such that the LUMO level of the

DOI: 10.1021/acsomega.8b01045
ACS Omega 2018, 3, 12893−12904

Table 1. Electrochemical Data for the Dyes 5a−b, 7c, and N719

Cpds	reduction[a] /V	oxidation[a] /V	E_{HOMO}[b] /eV	E_{LUMO}[b] /eV	band gap[c] /eV
5a	−1.94	0.73	−5.12	−2.45	2.67
5b	−1.74	0.67	−5.06	−2.65	2.41
7c	−2.29	0.64	−5.02	−2.10	2.92
N719	−2.04	0.46	−4.85	−2.35	2.50

[a]Measured in 1.0 mM solution of the dye in DMF with the addition of 0.1 M tetrabutylammonium tetrafluoroborate. Glassy carbon was used as a working electrode. Scan rate of potential: 0.01 V s^{-1}. Potentials (E) are indicated with respect to Fc^+/Fc. E_{pa} and E_{pc} stand for the potentials of anodic and cathodic peaks, respectively. [b]$E_{LUMO} = -(E_{red} + 4.39)$ (eV) and $E_{HOMO} = -(4.39 + E_{ox})$ (eV). [c]Calculated as the difference between the onset potentials of oxidation and reduction.

dye must be higher than that of the conduction band. Compound **5b** shows the lower LUMO level of all studied dyes (−2.65 eV), indicating the lowest thermodynamic driving force for electron injection. Compound **7c** exhibits the highest band gap among the compounds studied (2.92 eV), indicating that its photoexcitation is less efficient at long wavelengths—excitation requires higher energies. Even though the HOMO level is similar to that of compound **5b**, the LUMO level is much higher, which could be ascribed to the lower ability for electron capture by the carboxylic group present in **7c** when compared to the cyanoacetic moiety in **5b**.

2.3. Optical Studies. *2.3.1. Linear Optical Properties.* The absorption and emission spectra of heterocyclic compounds **3**−**7** were studied in ethanol, at room temperature. Table 2 summarizes the data, whereas Figure 1 displays the spectra of chromophores **4**−**7**. All of the push−pull chromophores studied exhibit at least one strong broad absorption band between 416 and 456 nm that is assigned to an ICT between the electron donor and acceptor groups. The peak of these absorption bands varies according to the spacer and electron-withdrawing moieties employed. The substitution of thieno[3,2-*b*]thiophene for the bithiophene moiety as the spacer induces a bathochromic shift in the longest wavelength absorption ($\Delta\lambda$ = 5 nm for compounds **3**, $\Delta\lambda$ = 30 nm for compounds **4**, $\Delta\lambda$ = 21 nm for compounds **5**, and $\Delta\lambda$ = 25 nm for compounds **6**) that is explained by the slight increase of the π-conjugation path and the enhanced auxiliary donor effect of bithiophene. Shifts of the absorption maxima are also observed when comparing the acceptor groups; generally, the higher the conjugation length and electron-withdrawing ability, the longer is the wavelength of maximum of absorption. For compounds **3** and **4**, the introduction of a formyl group leads to bathochromic shifts in the range of 42−67 nm. Comparing compounds **4** and **5**, the substitution of the formyl group for the 2-cyanoacetic acid moiety induces another bathochromic shift of 16−25 nm because of the stronger acceptor characteristics of the cyanoacetic group as well as the increase of conjugation. Comparison of compounds **4a**−**b** and **6a**−**b** shows that the dicyanovinyl group causes bathochromic shifts around 8−13 nm. Moreover, a hypsochromic shift of 24 nm is observed on comparing absorption spectra of compounds **4b** and **7c** because of the substitution of the electron-withdrawing formyl group by a carboxylic acid group. This result was not expected, bearing in mind the lower conjugation of the aldehyde compared to the carboxylic acid moiety. The novel cyanoacetic chromophores **5a**−**b** have high molar extinction coefficients (20 141−30 740 M^{-1} cm^{-1}) compared to the dicyanovinyl derivatives **6a**−**b** (19 221−26 766 M^{-1} cm^{-1}). Exciting compounds **3**−**7** at the maximum absorption wavelength, their emission spectra were recorded under room-temperature conditions (Figure 1, Table 2). The fluorescence was significantly influenced by the nature of the spacer and acceptor groups; generally, an increase in the extent of the π-conjugated system or functionalization with stronger electron donor or acceptor groups shifts the spectra to longer wavelengths. With the exception of compound **3b** (Φ_F = 0.20), all heterocyclic systems showed very weak emissive properties, with relative fluorescence quantum yields ranging from 0.01 to 0.03. When a nitrogen heteroatom is involved in the π-system, the n → π^* transition may be the lowest lying transition and is characterized by a radiative lifetime at least 100 times longer than that of low lying $\pi \rightarrow \pi^*$ transitions. Under these conditions, nonradiative processes are dominant, leading to low fluorescence quantum yields of many azo

Table 2. UV−Visible Absorption and Fluorescence Data for *N,N*-Diphenylhydrazone Derivatives 3−7 in Ethanol Solution at Room Temperature

	UV−vis	fluorescence			
Cpds	λ_{max}/nm	ε/M^{-1} cm^{-1}	λ_{em}/nm	Φ_F	Stokes shift/cm^{-1}
3a	368	24 867	428	0.03	3809
3b	373	26 060	454	0.20	4783
4a	410	29 750	480	0.01	3557
4b	440	23 588	536	0.01	4071
5a	435	30 740	519	0.01	3721
5b	456	20 141	574	0.03	4508
6a	423	26 766	564	0.01	5910
6b	448	19 221	591	0.01	5401
7c	416	12 562	501	0.01	4078

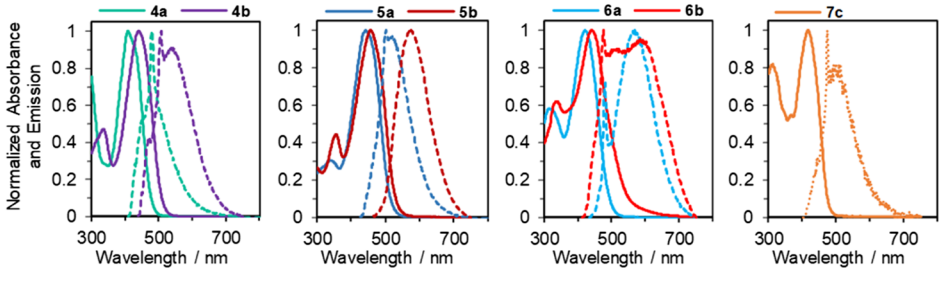

Figure 1. Normalized absorption (full solid lines) and emission (dashed lines) spectra for compounds **4**−**7** in ethanol at room temperature.

DOI: 10.1021/acsomega.8b01045
ACS Omega 2018, 3, 12893−12904

compounds as well as some compounds containing carbonyl groups and nitrogen heterocycles. As expected, a red shift of the emission of the compounds is observed upon increasing the strength of the acceptor group (aldehyde < carboxylic acid < cyanoacetic acid < dicyanovinyl). Thienothiophenes **4a**, **5a**, and **6a** show emissions at 480, 519, and 564 nm, respectively, whereas bithiophenes **4b**, **5b**, **6b**, and **7c** exhibit emissions at 536, 574, 591, and 501 nm, respectively. A bathochromic shift is also observed upon increasing the π-conjugation path length though the bithiophene spacer, comparing compound **4a** with **4b** (7 nm), compound **5a** with **5b** (52 nm), and compound **6a** with **6b** (18 nm). All of the studied push−pull systems show large Stokes' shifts (3557−5910 cm^{-1}), indicating that significant structure relaxation occurs in the excited state upon absorption. Moreover, the compounds functionalized with stronger electron-withdrawing cyanoacetic acid and dicyanovinyl moieties **5**−**6** exhibit larger Stokes' shifts than the corresponding aldehyde precursors **4**. This is consistent with the possibility of increased ICT upon absorption, particularly in the case of the dicyanovinyl moieties for which the Stokes shift increase is greater than 50%.

2.3.2. NLO Properties. Hyper-Rayleigh scattering[50,51] (HRS) was used to characterize the molecular first hyperpolarizabilities β of push−pull *N*,*N*-diphenylhydrazone derivatives **5**−**7**. The incident laser beam had a fundamental wavelength of 1064 nm, and the chromophores were dissolved in dioxane. The mean hyperpolarizability values, β, were determined by comparison with a *p*-nitroaniline (***p*NA**) reference solution.[52,53] The extent that the second harmonic signal might be contaminated by multiphoton-induced fluorescence was taken into account by measuring the HRS signal over different spectral bandwidths (see Supporting Information for more details). The static hyperpolarizabilities β_0 were estimated via a simple two-level model neglecting damping.[54−56] Both an increase in the π-conjugation of the spacer and an intensification of the electronic acceptor ability of the withdrawing group clearly influence the nonlinearities of compounds **4**−**7** as quantified in Table 3. First, the measured β values show that the bithiophene spacer leads to higher molecular hyperpolarizability values than the thieno[3,2-*b*]thiophene moiety. Therefore, aldehyde **4b** has a higher β value ($\beta = 290 \times 10^{-30}$ esu) than **4a** ($\beta = 205 \times 10^{-30}$ esu), as does cyanoacetic acid **5b** ($\beta = 2330 \times 10^{-30}$ esu) when compared to **5a** ($\beta = 930 \times 10^{-30}$ esu) and dicyanovinyl derivative **6b** ($\beta = 2750 \times 10^{-30}$ esu) in comparison with **6a** ($\beta = 265 \times 10^{-30}$ esu). The static hyperpolarizability β_0 values of the compounds follow the same trend. The more extensive π-conjugation and stronger auxiliary electron-donating ability of the bithiophene moiety are probably the main reasons for these trends. We also notice a general increase of the hyperpolarizability β as the electron-accepting ability is increased and as the electronic conjugation of the acceptor end moiety becomes larger. In the case of compounds bearing thieno[3,2-*b*]thiophene (**4a**, **5a**, and **6a**), the SHG response is enhanced by an increase of the acceptor group strength upon changing the aldehyde group ($\beta = 205 \times 10^{-30}$ esu for **4a**) to a dicyanovinyl group ($\beta = 265 \times 10^{-30}$ esu for **6a**) and then for a cyanoacetic acid moiety ($\beta = 930 \times 10^{-30}$ esu for **5a**). A similar tendency is observed in compounds bearing bithiophene as the spacer (**4b**, **5b**, **6b**, and **7c**). Derivative **4b** shows the lowest hyperpolarizability β, followed by the carboxylic acid **7c**. Chromophores **5b** and **6b** exhibit the highest values of β (2330×10^{-30} esu for **5b** and 2750×10^{-30} esu for **6b**); however, in this case, the dicyanovinyl derivative **6b** has higher SHG response than the cyanoacetic derivative **5b**. The lower hyperpolarizability β value of **5b** might be a result of the distorted conformation of the π-system due not only to the bithiophene spacer but also the cyanoacetic acid moiety when compared to the dicyanovinyl group. This could result in a suppression of electron transfer, even though the dominant conformer is planar between the spacer and acceptor moieties.[43] This result is in accordance with the electrochemical study of dyes **6**, previously reported by Roncali et al.,[23] where we noticed that the LUMO levels in dyes **6** do not follow the same trend as in dyes **5**: the introduction of the bithiophene spacer in dye **6b** leads to a destabilization of the LUMO (−3.45 eV for **6a** and −3.39 eV for **6b**), which is expected because of the stronger donating ability of the auxiliary electron, whereas in dye **5b**, the opposite occurs. The static hyperpolarisability β_0 values for the compounds show the same trend.

Table 3. UV−Vis Absorption Data in 1,4-Dioxane and β and β_0 Values for Chromophores 4−6 and 7c

	UV−vis[a]			
Cpds	λ_{max}/nm	$\varepsilon/M^{-1}\ cm^{-1}$	$\beta^b \times 10^{-30}$ esu	$\beta_0{}^c \times 10^{-30}$ esu
4a	408	30 871	205	72
4b	438	28 010	290	77
5a	464	31 534	930	180
5b	486	20 125	2330	300
6a	423	27 032	265	81
6b	447	20 022	2750	910
7c	422	12 444	370	114
***p*NA**	352		40.1	

[a]Wavelength of the absorption maximum of the respective compound when dissolved in dioxane. [b]Average hyperpolarizability values, β, reported in the T-convention. [c]Estimate of the static hyperpolarizability using the two-level model, $\beta_0 = \beta[1 - (\lambda_{max}/1064\ nm)^2][1 - (\lambda_{max}/532\ nm)^2]$, and neglecting damping factors.

2.4. Performance in DSSCs. Recently, several groups have reported that photovoltaic efficiencies ranged from 3.30 to 7.74% for organic hydrazine dyes bearing different π-spacers/electron donor groups (thiophene, pyrrole, furan, triphenylamino, and tetrahydroquinoline) and functionalized with various anchoring moieties (cyanoacetic acid and rhodanine acetic acid).[24−28] Therefore, we decided to expand these earlier studies as well as our work concerning organic sensitizers bearing bithiophene and thienothiophene spacers[42−45] to the synthesis of the novel bithiophene and thienothiophene dyes **5a**−**b** and **7c** to be evaluated as sensitizers for DSSCs.

Performance metrics of the DSSCs (efficiency—η, filling factor—FF, max. power point—MPP, voltage at open circuit—V_{OC}, current density at short-circuit—J_{SC}) sensitized with dyes **5a**−**b** and **7c** and **N719** reference dye, as well as the results from the coadsorption with deoxycholic acid (DCA) are presented in Table 4. The current−voltage characteristics of the prepared DSSCs are presented in Figure S1 (Supporting Information) and Figure 2 and show shapes typical for photodiodes for all of the cells. Incident photon-to-current conversion efficiency (IPCE) spectra are presented in Figure 3.

The DSSC prepared using *N*,*N*-diphenylhydrazone dye **7c** exhibits the lowest efficiency (0.72%). The very low J_{SC} (2.01 mA cm^{-2}) could be related to the low extinction coefficient

DOI: 10.1021/acsomega.8b01045
ACS Omega 2018, 3, 12893−12904

Table 4. Photovoltaic Parameters of the Cells Sensitized with Dyes 5a–b and 7c and N719 Reference Dye, as Well as Coadsorbed with DCA

sensitizer	V_{OC}/V	J_{SC}/mA cm^{-2}	MPP	FF	η/%
5a	0.64	6.41	2.67	0.67	2.98
5a + DCA	0.62	6.82	2.98	0.70	3.22
5b	0.61	6.77	2.78	0.67	3.01
5b + DCA	0.64	10.54	4.71	0.70	5.10
7c	0.54	2.01	0.67	0.62	0.72
7c + DCA	0.55	1.85	0.73	0.72	0.79
N719	0.74	16.11	8.51	0.72	9.25

(12562 M^{-1} cm^{-1}), narrow absorbance spectrum, and high electronic band gap (2.92 eV) exhibited by this dye. The IPCE spectra of the DSSC with **7c** dye supports these assumptions; only the higher energy photons from the spectral region 350–450 nm are able to turn the dye to its photoexcited state and contribute to photocurrent. However, this could turn to the advantage of this dye for "greenhouse" concept, where high transparency of the integrated photovoltaic device is eventually important.

DSSCs prepared using dyes **5a–b** show very similar photovoltaic efficiencies: 2.98% for **5a** and 3.01% for **5b**. The slightly higher efficiency of the DSSC sensitized with **5b** dye (about 33% of the efficiency of the DSSC with **N719** dye), bearing a bithiophene moiety as the π-spacer/auxiliary electron donor, results from the enhanced J_{SC} (6.77 mA cm^{-2}) that could be due to the longer π-conjugation of the sensitizing dye and lower electronic band gap when compared to dye **5a**.

To enhance the efficiency of the DSSCs sensitized with dyes **5a–b** and **7c**, we used coadsorption with DCA. Bile acids such as DCA and chenodeoxycholic acid are able to improve the efficiency of the cells because of the reduction of dye aggregation on the surface of TiO_2, suppressing dark current and improving electron lifetime.[25,57]

The photovoltaic response of the cells with dyes **5a** and **7c** was increased slightly by the addition of DCA as the coadsorbent (from 2.98 to 3.22% for dye **5a** and from 0.72 to 0.79% for dye **7c**), whereas the efficiency of the cell with dye **5b** improved significantly—from 3.01 to 5.10%. It can be seen from Table 4 and Figure 2 that the addition of DCA does not affect V_{OC} of the cells based on dyes **5a** and **7c**—the variations are within the statistical deviation. The slight enhancement of the performance of these cells is due to the improvement of the FF via suppressing the dark current. At the same time, for dye **5b**, coadsorption of DCA leads to noticeable increase of V_{OC}.

It is noteworthy that the addition of DCA to the sensitization solutions causes perceptible bathochromic shifts

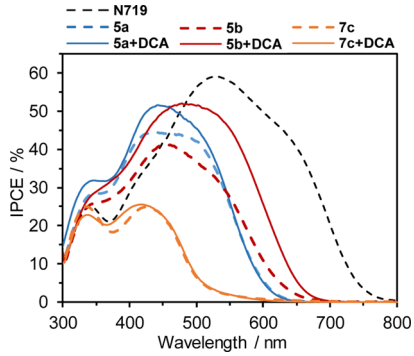

Figure 3. Spectra of IPCE for the cells assembled using **N719**, **5a–b**, and **7c** dyes. The sensitization was in 0.5 mM ethanol solutions of the corresponding dye (dashed lines) and with 50 mM DCA as an additive for coadsorption (solid lines).

in the transmittance and absorption spectra for dyes **5a–b** (Figure 4).

This bathochromic shift is accompanied by a slight increase of the quantum yield above 500 nm for the cell based on dye **5a**. Noteworthy, a pronounced improvement of quantum yield above 550 nm for the cell based on dye **5b** was observed (Figure 4). The overall performance of the DSSC with dye **5b** coadsorbed with DCA was found to be 5.01%, which is promising for metal-free organic dyes.

2.5. Computational Studies. The metal-free organic sensitizers **5a–b** and **7c** considered in our study have many possible conformations. Different conformers can have very different degrees of conjugation; therefore, it is important to determine the lowest energy conformers responsible for the observed absorption spectra of the dyes. For dyes **5a** and **5b**, 12 conformers were considered in each case, differing in the relative arrangements of the carboxylic acid, cyano, bithiophene (or thienothiophene), and *N*,*N*-diphenylhydrazone groups. For dye **7c**, we investigated the structures and energies of four different conformers. For dyes **5b** and **7c**, a simplification was introduced by considering only the thiophene–thiophene trans conformers. This is justified in view of previous studies,[43,58] which showed that the cis conformation usually accounts for ca. 10% of the population of conformers in this type of structures. Figure S2 (Supporting Information) shows the most stable conformers of these dyes and their relative energies calculated at the density functional theory (DFT) level. The energy differences found for these forms indicate a population of about 58% for conformer **5a-I**, 77% for conformer **5b-I**, and 53% for conformer **7c-I**. Because these are the dominant conformers, our subsequent analysis will be carried out for these forms, and for simplicity, we will

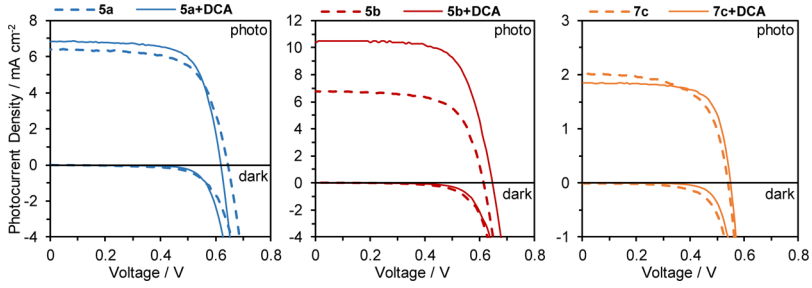

Figure 2. Current–voltage characteristics recorded under illumination and in the dark for the DSSCs assembled using synthesized dyes **5a–b** and **7c** (dashed lines) and with the DCA coadsorbent molecule.

DOI: 10.1021/acsomega.8b01045
ACS Omega 2018, 3, 12893–12904

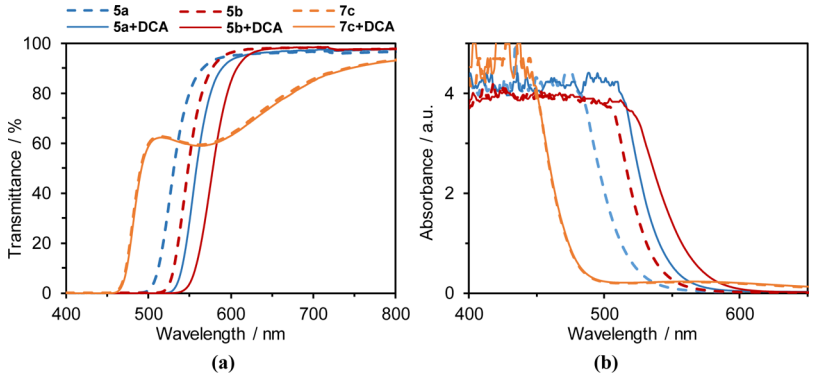

Figure 4. Transmittance (a) and absorbance (b) spectra for the ethanol solutions (0.5 mM) of the synthesized dyes **5a**–**b** and **7c** (dashed lines) and with the addition of 50 mM of DCA (solid lines).

refer to conformers **5a-I**, **5b-I**, and **7c-I** as dyes **5a**, **5b**, and **7c**, respectively.

Figure 5 presents the structures of the dominant conformers. In the three dyes, the cyano and the carboxylic groups are coplanar with the thienothiophene (in **5a**) or bithiophene (in **5b** and **7c**) π-bridges, showing strong conjugation between the π-orbitals of these groups. This is convenient because it will improve the efficiency of electron transfer from the bridge to the electron acceptor. Dye **7c** is slightly distorted in the region between the donor and the π-bridge.

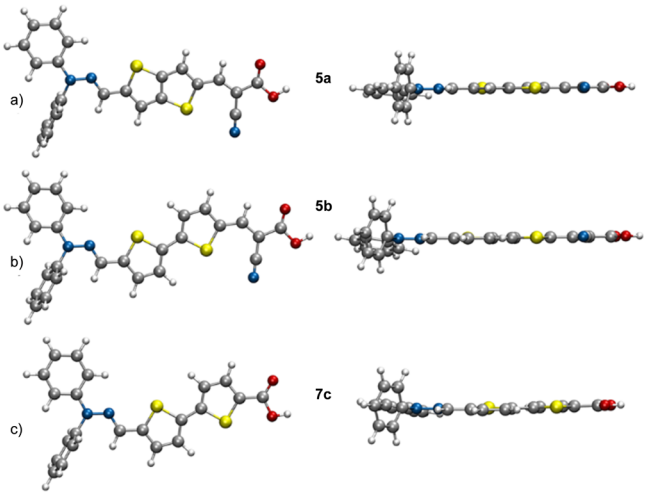

Figure 5. DFT B3LYP/6-31G(d,p) optimized geometries of conformers (a) **5a-I** (**5a**), (b) **5b-I** (**5b**), and (c) **7c-I** (**7c**).

Figure 6 shows the DFT-calculated energies for the frontier molecular orbitals of the three dyes. The larger extension of the conjugation in the chain in **5b** leads to a smaller band gap for this dye. Dye **7c** has the smallest conjugated chain, and for this reason, it has the highest band gap of the three dyes considered. This leads to a red shift of the first band in the absorption spectra of **5b** and a blue shift of the first band in the spectra of **7c**, compared with **5a**. The LUMO levels are significantly lower for **5a** and **5b**, compared with **7c**, in agreement with the cyanoacetic group being a better electron acceptor than the carboxylic one. The LUMO levels are above E_c of titania (−4.0 eV vs vacuum),[59] and the levels of HOMO are below the redox potential of $3I^-/I_3^-$ (−4.6 eV vs vacuum).[60] For utilizing in DSSCs, this means that the necessary driving force is provided for electron injection into the semiconductor and the regeneration of the dyes by the electrolyte. The data acquired from CV are provided in Figure 6 (green solid lines). One can see that HOMO and LUMO energies match very well the experimental CV values.

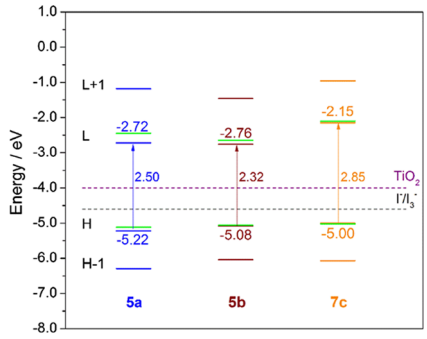

Figure 6. Energy of the frontier molecular orbitals calculated at the DFT B3LYP/6-31G(d,p) level of theory for the dyes **5a**, **5b**, and **7c**. The experimental values extracted from CV are marked with the green solid lines. The magenta dashed line points to the energy of the conduction band of TiO_2 (−4.0 eV for anatase), and the gray dashed line indicates the $3I^-/I_3^-$ redox potential (−4.6 eV). LUMO and HOMO are indicated as "L" and "H", respectively.

The UV–vis absorption spectra (vertical electronic excitations) were calculated for the free dyes at the time-dependent-DFT (TD-DFT)/CAM-B3LYP level, and the main contributions to the transitions with maximum absorption involve the HOMO − 1, HOMO, LUMO, and LUMO + 1 orbitals (Figure 7 and Table 5). For **5a**, the maximum absorption transition has a computed wavelength of 446 nm (experimental value 435 nm in ethanol) and corresponds predominantly to a HOMO → LUMO excitation (85%) with small contributions from HOMO − 1 → LUMO (8%) and HOMO → LUMO + 1 (3%) configurations. The maximum absorption of **5b** (calculated value is 470 nm and experimental value in ethanol is 456 nm) is red-shifted relatively to **5a**, as discussed above, and the dominant contributions to this transition are the HOMO → LUMO (79%), HOMO − 1 → LUMO (14%), and HOMO → LUMO + 1 (5%) excitations. Dye **7c** has its maximum absorption blue-shifted relative to **5a** and **5b**. The calculated maximum appears at 399 nm (in ethanol solvent, the experimental value is 416 nm), and as with dyes **5a** and **5b**, the main contribution is a HOMO → LUMO excitation (86%). From Figure 7, one can see the type of the orbitals involved in these transitions. The HOMOs are

DOI: 10.1021/acsomega.8b01045
ACS Omega 2018, 3, 12893−12904

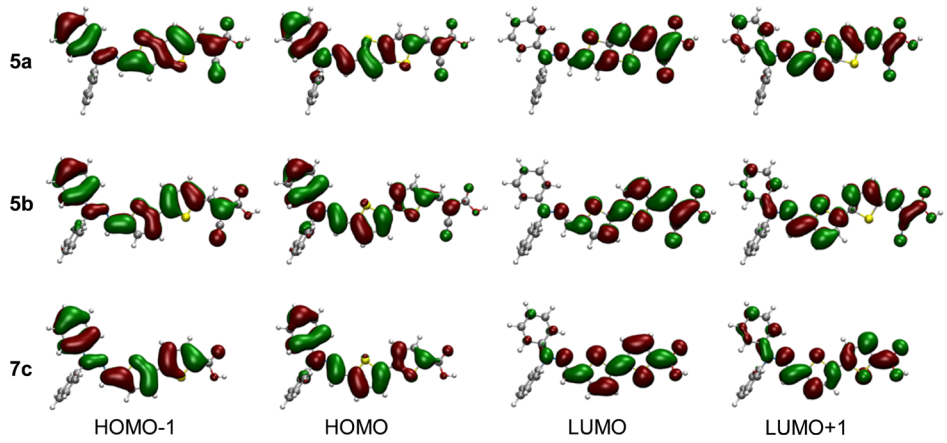

Figure 7. B3LYP/6-31G(d,p) frontier molecular orbitals of the free dyes **5a**, **5b**, and **7c**.

π orbitals, mainly localized on the donor and the thienothiophene (in **5a**) or bithiophene (in **5b** and **7c**) π-bridges, whereas the LUMOs are π^* orbitals essentially on the acceptor group and on the π-bridges. The HOMO − 1 → LUMO and HOMO → LUMO + 1 excitations tend to decrease the charge separation between the ground and excited states in these dyes; however, their contributions to the transition are very small. Therefore, there is efficient charge transfer between the donor and the acceptor upon excitation.

Adsorption of the dye on TiO_2 causes a reorganization of the electronic states of the semiconductor.[61−63] This can affect the electronic absorption spectra of the dyes and also the efficiency of injection of electrons into TiO_2. It is, therefore, important to evaluate the effect of adsorption of the dyes on their structural and electronic properties at the interface. Because of computational limitations, we only carried out this analysis for the dye **5a** adsorbed on TiO_2. Two types of approaches have been used to model the dye···TiO_2 interface. One is based on the simulation of the dye adsorbed to an infinitely large particle of TiO_2, in one or multiple dimensions, employing a periodic condition and using plane-wave basis sets. The second approach considers the dye adsorbed to an isolated cluster of $(TiO_2)_n$ and the calculations use a localized basis set.[61−68] Both methods present advantages, and in our study, we have used the second one. The size of the cluster, $(TiO_2)_9$, and the bidentate mode of adsorption in which the dye is covalently linked to a Ti atom of the cluster through the two oxygen atoms of the anchoring carboxylic group were also chosen based on the literature.[62,64,69,70] To keep electroneutrality of the system, the hydrogen atom coming from deprotonation[71] of the anchoring carboxylic group was linked to a cluster oxygen atom.[62,66] The geometry of the **5a**/TiO_2 system was optimized at the DFT level; the effect of dye adsorption on the energy levels of the orbitals is presented in Figure 8. The LUMO and the next virtual orbitals in the combined **5a**/TiO_2 system are stabilized relative to the same orbitals of the free dye. This is a consequence of the introduction of additional electronic states by the semiconductor. The HOMO and the next occupied orbitals are also slightly stabilized. Interestingly, however, there is no shift in the absorption maximum of the dye in the combined system, as we can see from Table 5. For the dye **5a** adsorbed to $(TiO_2)_9$, TD-DFT calculations estimate an absorption maximum at 446 nm, the same value as for the free dye. The maximum absorption transition in the combined **5a**/TiO_2 system has now significantly different contributions. Two dominant contributions come from the HOMO → LUMO (37%) and HOMO → LUMO + 3 (36%) excitations, together with minor contributions from HOMO → LUMO + 1 (4%), HOMO − 1 → LUMO (4%), HOMO → LUMO + 4 (4%), HOMO → LUMO + 6 (4%), and HOMO − 1 → LUMO + 3 (3%).

It should be noted that these energy gaps are different in the two systems. Smaller contributions come also from excitations with larger energy gaps, such as HOMO → LUMO + 25, HOMO → LUMO + 26, HOMO → LUMO + 27, and so forth, which are absent in the case of the free dye. The sum of all of these contributions in the case of **5a**/TiO_2 gives a resulting vertical excitation energy which is similar to one of the free dye.

Although their energy suffers slight changes, the HOMO and HOMO − 1 in the combined **5a**/TiO_2 system (Figure 9) are essentially equivalent to these orbitals in the free dye. In contrast, the LUMO and the remaining virtual orbitals involved in the maximum absorption transition are localized predominantly on the cluster. The LUMO + 3, LUMO + 4, and LUMO + 6 also extend to the acceptor and π-bridge. The distribution of electron density in these orbitals shows that there will be efficient electron injection from the excited dye into TiO_2 in a DSSC.

To discuss further the relation between the performance of the chromophores as sensitizers for TiO_2 DSSCs and their second-order NLO response, we focus on a comparison between compounds **5a** and **5b**. These chromophores differ only in their π-electron bridge and should have similar coupling efficiencies for electron transfer to the TiO_2 substrate. Given the tendency of many D−π−A molecules to form π-stacked aggregates on the surface of TiO_2 clusters, which will encourage the back transfer of electrons and, consequently, decrease DSSC efficiency, we further restrict our attention to the measurements using the coabsorber DCA, known for its ability to dissociate π-aggregates. The ratio of the efficiency of the **5b** + DCA DSSC to that of the **5a**−DCA DSSC is 5.10%:3.22% ≈ 1.6, roughly equal to the ratio of the extrapolated hyperpolarizabilities, 300:180 ≈ 1.7. Interestingly, the DFT-estimated oscillator strengths of the first singlet transition listed in Table 5 indicate that chromophore **5a** has a stronger dipole optical transition moment than chromophore **5b**. This suggests that the asymmetry in the optical field-induced polarizability of chromophore **5b** is greater, which

DOI: 10.1021/acsomega.8b01045
ACS Omega 2018, 3, 12893−12904

Table 5. TD-DFT/CAM-B3LYP Calculated Vertical Excitation Energies (E_{ex})[a], Absorption Maxima (λ_{max}), Main Contributions to the Excited State, and Oscillator Strengths (f) for Dyes 5a, 5b, and 7c

E_{ex}[a]/eV	λ_{max}/nm	λ_{max}[b]/nm	main contributions[c]/%	f
			Dye 5a	
2.78	446	435	H → L (85%), H − 1 → L (8%), H → L + 1 (3%)	1.747
			Dye 5a Adsorbed to $(TiO_2)_9$	
2.78	446		H → L (37%), H → L + 3 (36%), H → L + 1 (4%), H − 1 → L (4%), H → L + 4 (4%), H → L + 6 (4%), H − 1 → L + 3 (3%)	1.859
			Dye 5b	
2.64	470	456	H → L (79%), H − 1 → L (14%), H → L + 1 (5%)	1.546
			Dye 7c	
3.10	399	416	H → L (86%), H − 1 → L (7%), H → L + 1 (5%)	1.246

[a]Results from TD-DFT calculations at the CAM-B3LYP/6-311G(d,p) level of theory. [b]Experimental data from UV−vis spectra of the ethanolic solution. [c]Only the contributions ≥3% are indicated.

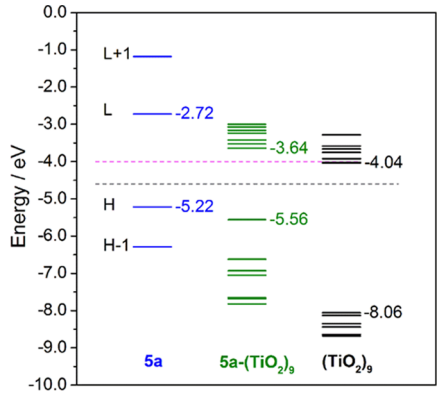

Figure 8. Energy of selected molecular orbitals calculated at the DFT B3LYP/6-31G(d,p) level of theory for the $(TiO_2)_9$ cluster and the dye **5a** adsorbed on $(TiO_2)_9$. The dashed line (magenta) points to the level of the conduction band edge of TiO_2 (−4.0 eV for anatase), and the gray dashed line indicates the $3I^-/I_3^-$ potential (4.6 eV). "L" and "H" stand for LUMO and HOMO, respectively.

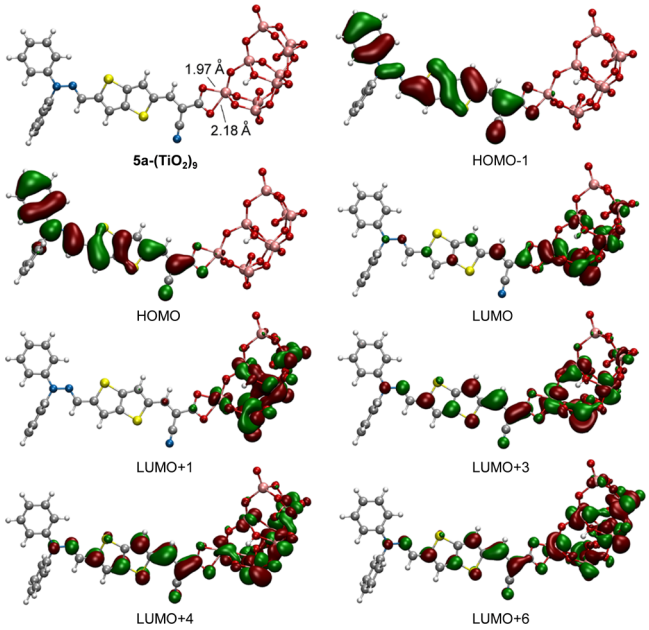

Figure 9. Optimized geometry and selected molecular orbitals of dye **5a** adsorbed on $(TiO_2)_9$ calculated at the B3LYP/6-31G(d,p) level.

might facilitate the transfer of photoexcited electrons from the donor to the substrate. We note that the DFT study carried out on chromophore **5a** coupled to a TiO_2 cluster indicated that because of the interaction between the chromophore and the substrate, the character of the first singlet transition changed; a substantial mixing of the LUMO + 3 state was accompanied by a strong reduction in the participation of the LUMO state (see Table 5). As the electron density of LUMO + 3 extends far into the π-bridge, this could result in less efficient electron collection by the substrate. The existence of a stronger charge-transfer asymmetry in chromophore **5b** might counteract this delocalization of the electron density from the TiO_2 cluster, promoting higher DSSC efficiencies.

3. CONCLUSIONS

N,*N*-Diphenylhydrazone derivatives **3**−**7** were obtained in fair to good yields, using commercially available precursors and

DOI: 10.1021/acsomega.8b01045
ACS Omega 2018, 3, 12893−12904

simple, convenient synthetic and purification procedures. Condensation of aldehydes **2a−c** with *N*,*N*-diphenylhydrazine gave intermediates **3a−b** and **7c**. Further functionalization of precursors **3a−b** through Vilsmeier formylation allowed the preparation of formyl derivatives **4a−b** that, through Knoevenagel condensation, gave the push−pull compounds **5−6**.

Experimental and theoretical characterization of the absorption, fluorescence, and NLO and electrochemical properties of the systems were carried out as a means to evaluate their potential as photosensitizers for nanocrystalline TiO_2-based DSSCs. The effect of different π-spacers and acceptor groups was evaluated. These comparative studies demonstrate that the incorporation the bithiophene π-bridge enhances the electron donor effect when compared with thienothiophene and that the dicyanovinyl acceptor group, although less conjugated than cyanoacetic acid and a weaker electron-withdrawing moiety, induces less distortion to the heterocyclic system, which can be advantageous.

Chromophores **5b** and **6b** exhibit the highest hyperpolarizability β (2330×10^{-30} esu for **5b**, 2750×10^{-30} esu for **6b**). The lower hyperpolarizability β value of **5b**, which is the more strongly conjugated system, could be attributed to the distorted conformation of the π-system due not only to the bithiophene spacer but also to the cyanoacetic acid moiety.

Compound **5b**, bearing a bithiophene π-spacer, exhibits the best conversion efficiency (3.01%) when used as a sensitizer for nanocrystalline titania in DSSCs because of the lower electronic band gap and longer π-conjugation of the sensitizing dye. Studies of coadsorption were performed by adding DCA to the sensitizing mixtures, revealing slight improvements for the cells based on dyes **5a** and **7c**, whereas the efficiency of the DSSCs with dye **5b** was significantly enhanced from 3.01 to 5.10%. This improvement originated from the bathochromic shift of the adsorption spectra of the dye **5b** in the presence of DCA and consequential widening of the spectral response of the photocurrent quantum yield.

Further optimization of the molecular structure of all chromophores should lead to enhanced hyperpolarizabilities and photovoltaic efficiencies.

4. EXPERIMENTAL SECTION

4.1. Materials and Methods. *N*,*N*-Diphenylhydrazine hydrochloride, 5-bromothiophene-2-carboxylic acid, thieno-[3,2-*b*]thiophene-2-carbaldehyde, 2,2′-bithiophene-5-carboxaldehyde, phosphorous oxychloride, malononitrile, and 2-cyanoacetic acid were obtained from Aldrich, whereas 5-formylthiopheneboronic acid was obtained from Acros Organics. All commercial reagents and solvents were used without further purification. The progress of the reaction was checked by means of thin-layer chromatography on 0.25 mm thick precoated silica plates (Merck Fertigplatten Kieselgel 60 F254); the spots were visualized using UV light. Silica gel column chromatography (Merck Kieselgel, 230−400 mesh) was used in the purification of the compounds. NMR spectra were performed on a Bruker Avance II 400 (working frequency of 400 MHz for ^{1}H and 100.6 MHz for ^{13}C), and the solvent peak was used as the internal reference. The solvents are specified in parenthesis before the chemical shifts values (δ relative to tetramethylsilane). Peak assignments were obtained by comparison of chemical shifts, peak multiplicities, and J values and were sustained by spin decoupling-double resonance and bidimensional heteronuclear multiple bond correlation and heteronuclear multiple quantum coherence techniques. Infrared spectra were obtained on a Bomem MB 104 spectrophotometer. UV−vis absorption spectra were recorded with a Shimadzu UV/2501PC spectrophotometer. Fluorescence spectra were obtained with a FluoroMax-4 spectrofluorometer, and relative fluorescence quantum yields were determined using the reference standard fluorescein in 0.1 M aqueous solution of NaOH (Φ_F = 0.79)[72] or 9,10-diphenylanthracene in ethanol.[73] Melting points were determined on a Gallenkamp machine. Mass spectra analysis was performed at the C.A.C.T.I.—Unidad de Espectrometria de Masas of the University of Vigo, Spain. The experimental procedures for the synthesis of precursor **2**, *N*,*N*-diphenylhydrazone derivatives **3a−b**, **7c**, aldehydes **4a−b**, the final push−pull cyanoacetic acid **5a−b**, and dicyanovinyl derivatives **6a−b** are described in the Supporting Information.

4.2. Cyclic Voltammetry. Autolab PGSTAT302N was used for electrochemical measurements. The measurements were performed in a three-electrode cell. Glassy carbon served as the working electrode, Pt was as the counter-electrode, and the reference was Ag/AgCl. Solutions were prepared using dry dimethylformamide (DMF). Concentrations of the dyes were 1 mM. $[NBu_4][BF_4]$ (0.1 M) was added to achieve sufficient conductivity. All solutions were deaerated by bubbling of N_2. As an internal redox reference, Fc^+/Fc was used.[42,74]

4.3. NLO Measurements. The orientationally averaged first hyperpolarizability β of the push−pull chromophores **4−7** was characterized by measuring the intensity of HRS provoked by incident q-switched laser pulses with a pulse duration of approximately 12 ns and an energy of 2 mJ. The experimental setup has been previously described[31,38] and is based on the pioneering work of Clays and Persoons,[50] (see Supporting Information for further details).

4.4. Preparation and Characterization of DSSCs. DSSCss were prepared as described in the Supporting Information. The photovoltaic performance was obtained with an Oriel Class solar simulator and a ZENNIUM workstation, using a metal mask with an aperture area of 0.25 cm^2, as previously reported.[42] (See Supporting Information for further details).

4.5. Computational Studies. DFT calculations were used to obtain the geometries and optoelectronic properties of the dyes **5a**, **5b**, and **7c**. The geometries of the free dyes were optimized with the B3LYP exchange correlation functional (combination of the hybrid exchange functional of Becke[75] together with the correlation functional LYP[76]), using the all-electron 6-31G(d,p) double-ζ plus polarization basis sets for all atoms. No symmetry constrains were imposed and the polarizable continuum model[77,78] was used to account for the effects of chloroform as the bulk solvent. The molecular structures of the most stable conformers of the dyes were also optimized with the CAM-B3LYP[79] functional. The harmonic vibrational frequencies were calculated to assess the nature of the optimized stationary points found in the potential energy surface and all were confirmed to be true minima (i.e., with no imaginary frequencies). The properties of the dye **5a** adsorbed to a $(TiO_2)_9$ cluster were also calculated. The initial geometry for the $(TiO_2)_9$ cluster was obtained from previous theoretical studies.[80,81] This structure was then optimized using the B3LYP functional and the Los Alamos effective core potential plus double-ζ basis set (LANL2DZ)[82−84] on titanium and the 6-31G(d,p) basis set for oxygen. The same computational procedure was used to optimize the geometry of the dye/TiO_2

DOI: 10.1021/acsomega.8b01045
ACS Omega 2018, 3, 12893−12904

combined system. TD-DFT calculations were carried out to analyze the absorption spectral properties of the free dyes and of the dye/TiO_2 system and also to calculate the vertical excitation energies for the lowest singlet excited states of the systems. The CAM-B3LYP[79] functional and the 6-311G(d,p) triple-ζ plus polarization basis sets were used in these calculations. The bulk solvent effects of chloroform were also considered in the TD-DFT calculations. All calculations were carried out using the GAMESS-US code.[85]

■ ASSOCIATED CONTENT

Supporting Information

The Supporting Information is available free of charge on the ACS Publications website at DOI: 10.1021/acsomega.8b01045.

Synthesis and characterization of compounds **3**−**6** and **7c**; experimental procedures concerning the synthesis; NLO measurements; preparation and evaluation of the performance of DSSCs and figures of optimized geometries and relative energies of the minima for dyes **5a**, **5b**, and **7c** [DFT B3LYP/6-31G(d,p)]; and photocurrent−voltage curves of the cells assembled using dyes **5a**−**b** and **7c** (PDF)

■ AUTHOR INFORMATION

Corresponding Author

*E-mail: mfox@quimica.uminho.pt. Phone: + 351 253 604381. Fax: + 351 253 604382 (M.M.M.R.).

ORCID

Licínia L. G. Justino: 0000-0002-8338-6441

M. Manuela M. Raposo: 0000-0002-7996-1626

Notes

The authors declare no competing financial interest.

■ ACKNOWLEDGMENTS

Thanks are due to Fundação para a Ciência e Tecnologia (FCT) for a PhD grant to S.S.M.F. (SFRH/BD/87786/2012). To FEDER-COMPETE for financial support through the research center CQUM (UID/QUI/0686/2016). The NMR spectrometers are part of the National NMR Network (PTNMR) and are partially supported by Infrastructure Project no. 022161 (cofinanced by FEDER through COMPETE 2020, POCI and PORL and FCT through PIDDAC). The group in Coimbra is grateful for funding from Centro de Química de Coimbra which is supported by the Fundação para a Ciência e a Tecnologia (FCT), Portuguese Agency for Scientific Research, through the programmes UID/QUI/UI0313/2013 and COMPETE. The authors also thank the Laboratory for Advanced Computing at the University of Coimbra for providing computing resources that have contributed to the research results reported in this manuscript. Thanks are also due to FCT for a postdoctoral grant to L.L.G.J. (SFRH/BPD/97026/2013). The group in Porto would like to acknowledge the European Commission through the Seventh Framework Programme, the Specific Programme "Ideas" of the European Research Council for research and technological development as part of an Advanced Grant under grant agreement no. 321315, which also partially funded this work. Some of this work was also performed under the project "SunStorage—Harvesting and storage of solar energy", with reference POCI-01-0145-FEDER-016387, funded by European Regional Development Fund (ERDF), through COMPETE 2020—Operational Programme for Competitiveness and Internationalization (OPCI), and by national funds, through FCT.

■ REFERENCES

(1) Bureš, F. Fundamental aspects of property tuning in push-pull molecules. *RSC Adv.* **2014**, *4*, 58826−58851.

(2) Klikar, M.; Solanke, P.; Tydlitát, J.; Bureš, F. Alphabet-inspired design of (hetero)aromatic push-pull chromophores. *Chem. Rec.* **2016**, *16*, 1886−1905.

(3) Allard, S.; Forster, M.; Souharce, B.; Thiem, H.; Scherf, U. Organic semiconductors for solution-processable field-effect transistors (OFETs). *Angew. Chem., Int. Ed.* **2008**, *47*, 4070−4098.

(4) Ohmori, Y. Development of organic light-emitting diodes for electro-optical integrated devices. *Laser Photonics Rev.* **2010**, *4*, 300−310.

(5) Burland, D. Optical nonlinearities in chemistry: introduction. *Chem. Rev.* **1994**, *94*, 1−2.

(6) He, G. S.; Tan, L.-S.; Zheng, Q.; Prasad, P. N. Multiphoton absorbing materials: molecular designs, characterizations, and applications. *Chem. Rev.* **2008**, *108*, 1245−1330.

(7) Pawlicki, M.; Collins, H. A.; Denning, R. G.; Anderson, H. L. Two-photon absorption and the design of two-photon dyes. *Angew. Chem., Int. Ed.* **2009**, *48*, 3244−3266.

(8) Hains, A. W.; Liang, Z.; Woodhouse, M. A.; Gregg, B. A. Molecular semiconductors in organic photovoltaic cells. *Chem. Rev.* **2010**, *110*, 6689−6735.

(9) Wu, Y.; Zhu, W. Organic sensitizers from D-π-A to D-A-π-A: effect of the internal electron-withdrawing units on molecular absorption, energy levels and photovoltaic performances. *Chem. Soc. Rev.* **2013**, *42*, 2039−2058.

(10) Clifford, J. N.; Martínez-Ferrero, E.; Viterisi, A.; Palomares, E. Sensitizer molecular structure-device efficiency relationship in dye sensitized solar cells. *Chem. Soc. Rev.* **2011**, *40*, 1635−1646.

(11) Mishra, A.; Bäuerle, P. Small molecule organic semiconductors on the move: promises for future solar energy technology. *Angew. Chem., Int. Ed.* **2012**, *51*, 2020−2067.

(12) Walker, B.; Kim, C.; Nguyen, T.-Q. Small molecule solution-processed bulk heterojunction solar cells. *Chem. Mater.* **2011**, *23*, 470−482.

(13) Duan, C.; Huang, F.; Cao, Y. Recent development of push-pull conjugated polymers for bulk-heterojunction photovoltaics: rational design and fine tailoring of molecular structures. *J. Mater. Chem.* **2012**, *22*, 10416−10434.

(14) Qian, G.; Wang, Z. Y. Near-infrared organic compounds and emerging applications. *Chem.—Asian J.* **2010**, *5*, 1006−1029.

(15) Singh, R. K.; Singh, A. K. DFT calculations on molecular structure, spectral analysis, multiple interactions, reactivity, NLO property and molecular docking study of flavanol-2,4-dinitrophenylhydrazone. *J. Mol. Structure* **2017**, *1129*, 128−141.

(16) Kwon, O.-P.; Jazbinsek, M.; Yun, H.; Seo, J.-I.; Kim, E.-M.; Lee, Y.-S.; Günter, P. Pyrrole-based hydrazone organic nonlinear optical crystals and their polymorphs. *Cryst. Growth Des.* **2008**, *8*, 4021−4025.

(17) Abbotto, A.; Beverina, L.; Manfredi, N.; Pagani, G. A.; Archetti, G.; Kuball, H.-G.; Wittenburg, C.; Heck, J.; Holtmann, J. Second-order nonlinear optical activity of dipolar chromophores based on pyrrole-hydrazono donor moieties. *Chem.—Eur. J.* **2009**, *15*, 6175−6185.

(18) Serbutoviez, C.; Bosshard, C.; Knoepfle, G.; Wyss, P.; Pretre, P.; Guenter, P.; Schenk, K.; Solari, E.; Chapuis, G. Hydrazone derivatives, an efficient class of crystalline materials for nonlinear optics. *Chem. Mater.* **1995**, *7*, 1198−1206.

(19) Lygaitis, R.; Getautis, V.; Grazulevicius, J. V. Hole-transporting hydrazones. *Chem. Soc. Rev.* **2008**, *37*, 770−788.

(20) Michaleviciūtė, A.; Lygaitis, R.; Gražulevičius, J. V.; Buika, G.; Jankauskas, V.; Undzėnas, A.; Fataraitė, E. Thiophene-based

DOI: 10.1021/acsomega.8b01045
ACS Omega 2018, 3, 12893−12904

hydrazones as hole-transporting materials. *Synth. Met.* **2009**, *159*, 223−227.
(21) Sassi, M.; Crippa, M.; Ruffo, R.; Turrisi, R.; Drees, M.; Pandey, U. K.; Termine, R.; Golemme, A.; Facchetti, A.; Beverina, L. Open circuit voltage tuning through molecular design in hydrazone end capped donors for bulk heterojunction solar cells. *J. Mater. Chem. A* **2013**, *1*, 2631−2638.
(22) Silvestri, F.; Irwin, M. D.; Beverina, L.; Facchetti, A.; Pagani, G. A.; Marks, T. J. Efficient squaraine-based solution processable bulk-heterojunction solar Cells. *J. Am. Chem. Soc.* **2008**, *130*, 17640−17641.
(23) Diac, A.; Demeter, D.; Allain, M.; Grosu, I.; Roncali, J. Simple and versatile molecular donors for organic photovoltaics prepared by metal-free synthesis. *Chem.—Eur. J.* **2015**, *21*, 1598−1608.
(24) Urnikaite, S.; Daskeviciene, M.; Send, R.; Wonneberger, H.; Sackus, A.; Bruder, I.; Getautis, V. Organic dyes containing a hydrazone moiety as auxiliary donor for solid-state DSSC applications. *Dyes Pigm.* **2015**, *114*, 175−183.
(25) Shen, P.; Liu, X.; Jiang, S.; Huang, Y.; Yi, L.; Zhao, B.; Tan, S. Effects of aromatic π-conjugated bridges on optical and photovoltaic properties of *N*,*N*-diphenylhydrazone-based metal-free organic dyes. *Org. Electron.* **2011**, *12*, 1992−2002.
(26) Shen, P.; Liu, X.; Jiang, S.; Wang, L.; Yi, L.; Ye, D.; Zhao, B.; Tan, S. Synthesis of new *N*,*N*-diphenylhydrazone dyes for solar cells: Effects of thiophene-derived π-conjugated bridge. *Dyes Pigm.* **2012**, *92*, 1042−1051.
(27) Rakstys, K.; Solovjova, J.; Malinauskas, T.; Bruder, I.; Send, R.; Sackus, A.; Sens, R.; Getautis, V. A structural study of 1-phenyl-1,2,3,4-tetrahydroquinoline-based dyes for solid-state DSSC applications. *Dyes Pigm.* **2014**, *104*, 211−219.
(28) Urnikaite, S.; Malinauskas, T.; Bruder, I.; Send, R.; Gaidelis, V.; Sens, R.; Getautis, V. Organic dyes with hydrazone moieties: a study of correlation between structure and performance in the solid-state dye-sensitized solar cells. *J. Phys. Chem. C* **2014**, *118*, 7832−7843.
(29) Cinar, M. E.; Ozturk, T. Thienothiophenes, dithienothiophenes, and thienoacenes: syntheses, oligomers, polymers, and properties. *Chem. Rev.* **2015**, *115*, 3036−3140.
(30) Mishra, A.; Ma, C.-Q.; Bäuerle, P. Functional oligothiophenes: molecular design for multidimensional nanoarchitectures and their applications. *Chem. Rev.* **2009**, *109*, 1141−1276.
(31) Raposo, M. M. M.; Sousa, A. M. R. C.; Kirsch, G.; Cardoso, P.; Belsley, M.; de Matos Gomes, E.; Fonseca, A. M. C. Synthesis and characterization of dicyanovinyl-substituted thienylpyrroles as new nonlinear optical chromophores. *Org. Lett.* **2006**, *8*, 3681−3684.
(32) Batista, R. M. F.; Costa, S. P. G.; Belsley, M.; Lodeiro, C.; Raposo, M. M. M. Synthesis and characterization of novel (oligo)thienyl-imidazo-phenanthrolines as versatile π-conjugated systems for several optical applications. *Tetrahedron* **2008**, *64*, 9230−9238.
(33) Raposo, M. M. M.; Herbivo, C.; Hugues, V.; Clermont, G.; Castro, M. C. R.; Comel, A.; Blanchard-Desce, M. Synthesis, fluorescence, and two-photon absorption properties of push-pull 5-arylthieno[3,2-*b*]thiophene derivatives. *Eur. J. Org. Chem.* **2016**, 5263−5273.
(34) Raposo, M. M. M.; Castro, M. C. R.; Belsley, M.; Fonseca, A. M. C. Push-pull bithiophene azo-chromophores bearing thiazole and benzothiazole acceptor moieties: Synthesis and evaluation of their redox and nonlinear optical properties. *Dyes Pigm.* **2011**, *91*, 454−465.
(35) Genin, E.; Hugues, V.; Clermont, G.; Herbivo, C.; Castro, M. C. R.; Comel, A.; Raposo, M. M. M.; Blanchard-Desce, M. Fluorescence and two-photon absorption of push-pull aryl(bi)-thiophenes: structure-property relationships. *Photochem. Photobiol. Sci.* **2012**, *11*, 1756−1766.
(36) Castro, M. C. R.; Schellenberg, P.; Belsley, M.; Fonseca, A. M. C.; Fernandes, S. S. M.; Raposo, M. M. M. Design, synthesis and evaluation of redox, second order nonlinear optical properties and theoretical DFT studies of novel bithiophene azo dyes functionalized with thiadiazole acceptor groups. *Dyes Pigm.* **2012**, *95*, 392−399.
(37) Wojciechowski, A.; Raposo, M. M. M.; Castro, M. C. R.; Kuznik, W.; Fuks-Janczarek, I.; Pokladko-Kowar, M.; Bureš, F. Nonlinear optoelectronic materials formed by push-pull (bi)-thiophene derivatives functionalized with di(tri)cyanovinyl acceptor groups. *J. Mater. Sci.: Mater. Electron.* **2014**, *25*, 1745−1750.
(38) Castro, M. C. R.; Belsley, M.; Raposo, M. M. M. Synthesis and characterization of push-pull bithienylpyrrole NLOphores with enhanced hyperpolarizabilities. *Dyes Pigm.* **2016**, *131*, 333−339.
(39) Mohammed, N.; Wiles, A. A.; Belsley, M.; Fernandes, S. S. M.; Cariello, M.; Rotello, V. M.; Raposo, M. M. M.; Cooke, G. Synthesis and characterisation of push-pull flavin dyes with efficient second harmonic generation (SHG) properties. *RSC Adv.* **2017**, *7*, 24462−24469.
(40) Fernandes, S. S. M.; Herbivo, C.; Aires-de-Sousa, J.; Comel, A.; Belsley, M.; Raposo, M. M. M. Theoretical and experimental studies of aryl-bithiophene based push-pull π-conjugated heterocyclic systems bearing cyanoacetic or rhodanine-3-acetic acid acceptors for SHG nonlinear optical applications. *Dyes Pigm.* **2018**, *149*, 566−573.
(41) Fernandes, S. S. M.; Belsley, M.; Ciarrocchi, C.; Licchelli, M.; Raposo, M. M. M. Terpyridine derivatives functionalized with (hetero)aromatic groups and the corresponding Ru complexes: Synthesis and characterization as SHG chromophores. *Dyes Pigm.* **2018**, *150*, 49−58.
(42) Fernandes, S. S. M.; Castro, M. C. R.; Mesquita, I.; Andrade, L.; Mendes, A.; Raposo, M. M. M. Synthesis and characterization of novel thieno[3,2-*b*]thiophene based metal-free organic dyes with different heteroaromatic donor moieties as sensitizers for dye-sensitized solar cells. *Dyes Pigm.* **2017**, *136*, 46−53.
(43) Fernandes, S. S. M.; Mesquita, I.; Andrade, L.; Mendes, A.; Justino, L. L. G.; Burrows, H. D.; Raposo, M. M. M. Synthesis and characterization of push-pull bithiophene and thieno[3,2-*b*]thiophene derivatives bearing an ethyne linker as sensitizers for dye-sensitized solar cells. *Org. Electron.* **2017**, *49*, 194−205.
(44) Fernandes, S. S. M.; Castro, M. C. R.; Pereira, A. I.; Mendes, A.; Serpa, C.; Pina, J.; Justino, L. L. G.; Burrows, H. D.; Raposo, M. M. M. Optical and Photovoltaic properties of thieno[3,2-*b*]-thiophene-based push-pull organic dyes with different anchoring groups for dye-sensitized solar cells. *ACS Omega* **2017**, *2*, 9268−9279.
(45) Fernandes, S. S. M.; Pereira, A.; Ivanou, D.; Mendes, A.; Raposo, M. M. M. Benzothiadiazole derivatives functionalized with two different (hetero)aromatic donor groups: Synthesis and evaluation as TiO_2 sensitizers for DSSCs. *Dyes Pigm.* **2018**, *151*, 89−94.
(46) Liu, H.; Wu, F.; Zhao, B.; Meng, L.; Wang, G.; Zhang, J.; Shen, P.; Tan, S. Synthesis and photovoltaic properties of the acceptor pended push-pull conjugated polymers incorporating thieno[3,2-*b*] thiophene in the backbone chain or side chains. *Dyes Pigm.* **2015**, *120*, 44−51.
(47) Zhu, S.; An, Z.; Sun, X.; Wu, Z.; Chen, X.; Chen, P. Synthesis and evaluation of simple molecule as a co-adsorbent dye for highly efficient co-sensitized solar cells. *Dyes Pigm.* **2015**, *120*, 85−92.
(48) Hagfeldt, A.; Graetzel, M. Light-induced redox reactions in nanocrystalline systems. *Chem. Rev.* **1995**, *95*, 49−68.
(49) Mikroyannidis, J. A.; Roy, M. S.; Sharma, G. D. Synthesis of new low band gap dyes with BF2-azopyrrole complex and their use for dye-sensitized solar cells. *J. Power Sources* **2010**, *195*, 5391−5398.
(50) Clays, K.; Persoons, A. Hyper-Rayleigh scattering in solution. *Rev. Sci. Instrum.* **1992**, *63*, 3285−3289.
(51) Clays, K.; Persoons, A. Hyper-Rayleigh scattering in solution. *Phys. Rev. Lett.* **1991**, *66*, 2980−2983.
(52) Reis, H. Problems in the comparison of theoretical and experimental hyperpolarizabilities revisited. *J. Chem. Phys.* **2006**, *125*, 014506.
(53) Kaatz, P.; Shelton, D. P. Polarized hyper-Rayleigh light scattering measurements of nonlinear optical chromophores. *J. Chem. Phys.* **1996**, *105*, 3918−3929.
(54) Oudar, J. L. Optical nonlinearities of conjugated molecules. Stilbene derivatives and highly polar aromatic compounds. *J. Chem. Phys.* **1977**, *67*, 446−457.

DOI: 10.1021/acsomega.8b01045
ACS Omega 2018, 3, 12893−12904

(55) Oudar, J. L.; Chemla, D. S. Hyperpolarizabilities of the nitroanilines and their relations to the excited state dipole moment. *J. Chem. Phys.* **1977**, *66*, 2664−2668.
(56) Oudar, J. L.; Zyss, J. Structural dependence of nonlinear-optical properties of methyl-(2,4-dinitrophenyl)-aminopropanoate crystals. *Phys. Rev. A: At. Mol. Opt. Phys.* **1982**, *26*, 2016−2027.
(57) Wang, Z.-S.; Cui, Y.; Dan-oh, Y.; Kasada, C.; Shinpo, A.; Hara, K. Thiophene-functionalized coumarin dye for efficient dye-sensitized solar cells: electron lifetime improved by coadsorption of deoxycholic acid. *J. Phys. Chem. C* **2007**, *111*, 7224−7230.
(58) Al-Eid, M.; Lim, S.; Park, K.-W.; Fitzpatrick, B.; Han, C.-H.; Kwak, K.; Hong, J.; Cooke, G. Facile synthesis of metal-free organic dyes featuring a thienylethynyl spacer for dye sensitized solar cells. *Dyes Pigm.* **2014**, *104*, 197−203.
(59) Grätzel, M. Photoelectrochemical cells. *Nature* **2001**, *414*, 338−344.
(60) Zhang, G.; Bai, Y.; Li, R.; Shi, D.; Wenger, S.; Zakeeruddin, S. M.; Grätzel, M.; Wang, P. Employ a *bis*thienothiophene linker to construct an organic chromophore for efficient and stable dye-sensitized solar cells. *Energy Environ. Sci.* **2009**, *2*, 92−95.
(61) Sánchez-de-Armas, R.; Oviedo, J.; San Miguel, M. Á.; Sanz, J. F. Direct *vs* indirect mechanisms for electron injection in dye-sensitized solar cells. *J. Phys. Chem. C* **2011**, *115*, 11293−11301.
(62) Sánchez-de-Armas, R.; Oviedo López, J.; San-Miguel, M. A.; Sanz, J. F.; Ordejón, P.; Pruneda, M. Real-time TD-DFT simulations in dye sensitized solar cells: the electronic absorption spectrum of alizarin supported on TiO_2 nanoclusters. *J. Chem. Theory Comput.* **2010**, *6*, 2856−2865.
(63) Sánchez-de-Armas, R.; San-Miguel, M. A.; Oviedo, J.; Márquez, A.; Sanz, J. F. Electronic structure and optical spectra of catechol on TiO_2 nanoparticles from real time TD-DFT simulations. *Phys. Chem. Chem. Phys.* **2011**, *13*, 1506−1514.
(64) Zhang, L.; Cole, J. M.; Dai, C. Variation in optoelectronic properties of azo dye-sensitized TiO_2 semiconductor interfaces with different adsorption anchors: carboxylate, sulfonate, hydroxyl and pyridyl groups. *ACS Appl. Mater. Interfaces* **2014**, *6*, 7535−7546.
(65) Liang, J.; Zhu, C.; Cao, Z. Electronic and optical properties of the triphenylamine-based organic dye sensitized TiO_2 semiconductor: insight from first principles calculations. *Phys. Chem. Chem. Phys.* **2013**, *15*, 13844−13851.
(66) Sánchez-de-Armas, R.; San Miguel, M. Á.; Sanz, J. F. Coumarin derivatives for dye sensitized solar cells: a TD-DFT study. *Phys. Chem. Chem. Phys.* **2012**, *14*, 225−233.
(67) Anselmi, C.; Mosconi, E.; Pastore, M.; Ronca, E.; De Angelis, F. Adsorption of organic dyes on TiO_2 surfaces in dye-sensitized solar cells: interplay of theory and experiment. *Phys. Chem. Chem. Phys.* **2012**, *14*, 15963−15974.
(68) Ronca, E.; Pastore, M.; Belpassi, L.; Tarantelli, F.; De Angelis, F. Influence of the dye molecular structure on the TiO_2 conduction band in dye-sensitized solar cells: disentangling charge transfer and electrostatic effects. *Energy Environ. Sci.* **2013**, *6*, 183−193.
(69) Hara, K.; Sato, T.; Katoh, R.; Furube, A.; Yoshihara, T.; Murai, M.; Kurashige, M.; Ito, S.; Shinpo, A.; Suga, S.; Arakawa, H. Novel conjugated organic dyes for efficient dye-sensitized solar cells. *Adv. Funct. Mater.* **2005**, *15*, 246−252.
(70) Wang, Q.; Campbell, W. M.; Bonfantani, E. E.; Jolley, K. W.; Officer, D. L.; Walsh, P. J.; Gordon, K.; Humphry-Baker, R.; Nazeeruddin, M. K.; Grätzel, M. Efficient light harvesting by using green Zn-porphyrin-sensitized nanocrystalline TiO_2 films. *J. Phys. Chem. B* **2005**, *109*, 15397−15409.
(71) Wang, Z.-S.; Hara, K.; Dan-oh, Y.; Kasada, C.; Shinpo, A.; Suga, S.; Arakawa, H.; Sugihara, H. Photophysical and (photo)-electrochemical properties of a coumarin dye. *J. Phys. Chem. B* **2005**, *109*, 3907−3914.
(72) Umberger, J. Q.; LaMer, V. K. The kinetics of diffusion controlled molecular and ionic reactions in solution as determined by measurements of the quenching of fluorescence. *J. Am. Chem. Soc.* **1945**, *67*, 1099−1109.
(73) Morris, J. V.; Mahaney, M. A.; Huber, J. R. Fluorescence quantum yield determinations. 9,10-Diphenylanthracene as a reference standard in different solvents. *J. Phys. Chem.* **1976**, *80*, 969−974.
(74) Cardona, C. M.; Li, W.; Kaifer, A. E.; Stockdale, D.; Bazan, G. C. Electrochemical considerations for determining absolute frontier orbital energy levels of conjugated polymers for solar cell applications. *Adv. Mater.* **2011**, *23*, 2367−2371.
(75) Becke, A. D. Density-functional thermochemistry. III. The role of exact exchange. *J. Chem. Phys.* **1993**, *98*, 5648−5652.
(76) Lee, C.; Yang, W.; Parr, R. G. Development of the Colle-Salvetti correlation-energy formula into a functional of the electron density. *Phys. Rev. B: Condens. Matter Mater. Phys.* **1988**, *37*, 785−789.
(77) Miertuš, S.; Scrocco, E.; Tomasi, J. Electrostatic interaction of a solute with a continuum. A direct utilizaion of AB initio molecular potentials for the prevision of solvent effects. *Chem. Phys.* **1981**, *55*, 117−129.
(78) Tomasi, J.; Mennucci, B.; Cammi, R. Quantum mechanical continuum solvation models. *Chem. Rev.* **2005**, *105*, 2999−3094.
(79) Yanai, T.; Tew, D. P.; Handy, N. C. A new hybrid exchange-correlation functional using the Coulomb-attenuating method (CAM-B3LYP). *Chem. Phys. Lett.* **2004**, *393*, 51−57.
(80) Qu, Z.-w.; Kroes, G.-J. Theoretical study of the electronic structure and stability of titanium dioxide clusters $(TiO_2)_n$ with n = 1−9. *J. Phys. Chem. B* **2006**, *110*, 8998−9007.
(81) Hamad, S.; Catlow, C. R. A.; Woodley, S. M.; Lago, S.; Mejías, J. A. Structure and stability of small TiO_2 nanoparticles. *J. Phys. Chem. B* **2005**, *109*, 15741−15748.
(82) Hay, P. J.; Wadt, W. R. Ab initio effective core potentials for molecular calculations. Potentials for the transition metal atoms Sc to Hg. *J. Chem. Phys.* **1985**, *82*, 270−283.
(83) Hay, P. J.; Wadt, W. R. Ab initio effective core potentials for molecular calculations. Potentials for K to Au including the outermost core orbitals. *J. Chem. Phys.* **1985**, *82*, 299−310.
(84) Wadt, W. R.; Hay, P. J. Ab initio effective core potentials for molecular calculations. Potentials for main group elements Na to Bi. *J. Chem. Phys.* **1985**, *82*, 284−298.
(85) Schmidt, M. W.; Baldridge, K. K.; Boatz, J. A.; Elbert, S. T.; Gordon, M. S.; Jensen, J. H.; Koseki, S.; Matsunaga, N.; Nguyen, K. A.; Su, S.; Windus, T. L.; Dupuis, M.; Montgomery, J. A. General atomic and molecular electronic structure system. *J. Comput. Chem.* **1993**, *14*, 1347−1363.

DOI: 10.1021/acsomega.8b01045
ACS Omega 2018, 3, 12893−12904